



Identification of visible lines from multiply charged W^{8+} and W^{9+} ions

Priti ^{1,*}, Momoe Mita,¹ Daiji Kato ^{2,3}, Izumi Murakami,^{2,4} Hiroyuki A. Sakaue,² and Nobuyuki Nakamura¹

¹*Institute for Laser Science, The University of Electro-Communications, Tokyo 182-8585, Japan*

²*National Institute for Fusion Science, National Institutes of Natural Sciences, Toki, Gifu 509-5292, Japan*

³*Department of Advanced Energy Engineering Science, Kyushu University, Fukuoka 816-8580, Japan*

⁴*Department of Fusion Science, The Graduate University for Advanced Studies, SOKENDAI, Toki, Gifu 509-5292, Japan*



(Received 17 August 2020; accepted 2 October 2020; published 23 October 2020)

We present an investigation of previously unidentified visible lines for W^{8+} and W^{9+} from the spectra observed using an electron-beam ion trap. The analysis is based on collisional-radiative (CR) modeling with fine-structure sublevel population kinetics. To ensure the identification of lines done by the CR model, we have also performed an accurate calculation of transition energies and transition probabilities within the multiconfigurational Dirac-Fock approach using GRASP2018. In the spectrum, most of the observed lines are assigned as magnetic dipole transitions belonging to the first two lower-lying configurations of these ions.

DOI: [10.1103/PhysRevA.102.042818](https://doi.org/10.1103/PhysRevA.102.042818)

I. INTRODUCTION

Understanding the spectra from the lower charged states of tungsten is essential due to its application in several fields. In particular, tungsten is planned to be used as a plasma-facing component in the ITER divertor [1]. The temperature of the divertor plasma is expected to be a few hundred eV, and in this temperature range the most abundant tungsten charged states are W^{1+} to W^{15+} [2,3]. Therefore, there will be a high possibility of observing UV and visible lines from these charge states from the ITER divertor region, which can be used in the divertor plasma diagnostics [4]. Especially, spectral studies of W^{7+} to W^{13+} ions are challenging as these ions have very complex atomic structures with the open $4f$ subshell, and competition of orbital energies between $4f$, $5s$, and $5p$ electrons. For example, the one-electron Dirac-Fock (DF) energies of the $4f$, $5s$, and $5p$ orbitals as a function of Z for a Dy-like isoelectronic sequence (66 electrons) are calculated by GRASP2018 [5] and shown in Fig. 1. It shows that around $Z = 74$, i.e., W^{8+} , there is a considerable overlap of $5p$ and $4f$ orbital energies which results in the competition between $4f^{14}5s^25p^4$ and $4f^{13}5s^25p^5$ energy levels for the ground state. Due to such level crossing Berengut *et al.* [6,7] have proposed forbidden transitions in W^{7+} and W^{8+} as prospective candidates for next-generation atomic clocks sensitive to variation in fine-structure constant. Not only are spectral studies of these ions important for their applications, but they are also essential to test the limit of the existing theoretical methods.

To date, several studies are available on highly charged tungsten ions as the corresponding atomic systems (few electrons) are relatively simple. However, there is still a big void for lower charged tungsten ions from W^{7+} to W^{13+} , as pointed out by Ralchenko [8] and in data compiled by

Kramida and Shirai [9]. In recent years, a couple of theoretical and experimental works have been reported for W^{7+} ions. Berengut *et al.* [6] reported the energies for four levels from configuration-interaction (CI) calculations, which match the level sequence reported by Kramida and Shirai [9]. Ryabtsev *et al.* [10,11] observed the spectrum from vacuum spark plasma and confirmed the ground state to be $4f^{13}5p^6$. Furthermore, the fine-structure splitting of the ground term $4f^{13}5p^6\ 2F_{5/2,7/2}$ was measured by direct observation of the magnetic dipole (M1) line with a compact electron-beam ion trap (CoBIT) in Tokyo by Mita *et al.* [12]. The fine-structure splitting was also measured by Lu *et al.* [13]. Spectra of W^{11+} – W^{15+} in the 17–26-nm region and a visible line from W^{11+} were measured from a compact electron-beam ion trap (EBIT) in Shanghai (SH-HtscEBIT) [14]. In the visible range, 365–475-nm lines from charged states 8–28 were observed by Komatsu *et al.* [15] using CoBIT. However, for W^{8+} to W^{10+} ions, spectral data are still scarce, and no data are available in the Atomic Spectra Database of the NIST [16]. Only for W^{8+} , the 16 lowest-energy levels from $4f^{14}5s^25p^4$, $4f^{13}5s^25p^5$, and $4f^{12}5s^25p^6$ were theoretically calculated from FAC by Berengut *et al.* [6]. For W^{9+} and W^{10+} , no theoretical or experimental results are reported for energy levels or spectral lines.

To fill this void low charged tungsten ions (W^{6+} – W^{13+}) were produced and trapped in CoBIT [12,17] previously. EUV spectra were recorded for W^{7+} – W^{13+} and visible spectra were recorded for W^{7+} – W^{9+} . However, in the visible range, only the line from the M1 transition between the fine-structure splitting of the ground configuration of W^{7+} was assigned while other lines presented in the spectra were unidentified. Therefore, in the present paper, we analyze and identify the additional lines from W^{8+} and W^{9+} ions with detailed collisional-radiative (CR) model calculations. To aid the identification's reliability, we have also performed a structure calculation for these ions within the multiconfiguration Dirac-Fock (MCDF) approach using GRASP2018 [5].

*priti@ils.uec.ac.jp

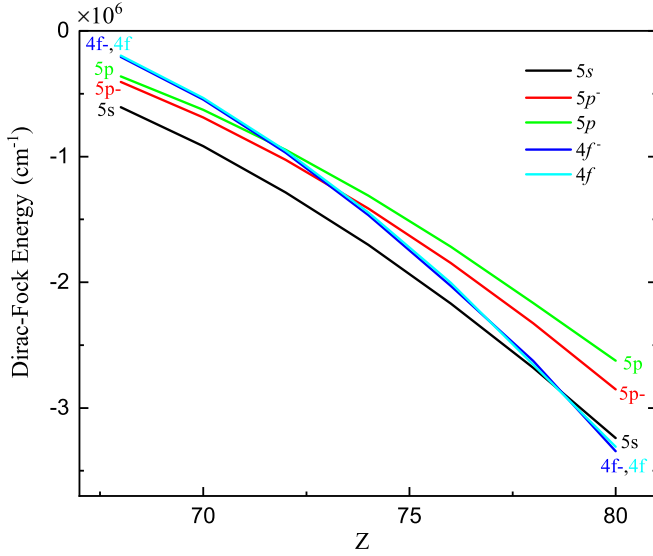


FIG. 1. Dirac-Fock energies of a Dy-like isoelectronic ($N = 66$) sequence calculated by GRASP2018.

II. EXPERIMENT

The experiment was performed by using a CoBIT [18] at the University of Electro-Communications. For the details of the experimental setup, see our previous papers [12,19]. Briefly, multiply charged tungsten ions were produced in CoBIT, consisting of an electron gun, a drift tube, an electron collector, and a high-critical-temperature superconducting magnet. The drift tube is composed of three successive cylindrical electrodes that act as an ion trap by applying a positive potential (typically 30 V) at both ends with respect to the middle electrode. The electron beam emitted from the electron gun is accelerated towards the drift tube while it is compressed by the axial magnetic field (typically 0.08 T) produced by the magnet surrounding the drift tube. The electron-beam current was 3 to 5 mA depending on the electron-beam energy. Tungsten was continuously introduced into the trap through a gas injector as a vapor of $W(CO)_6$. In order to maintain a good charge state distribution, the injection flow rate was carefully controlled by using a variable leak valve. Since there are no possible contaminating elements that are heavier than tungsten, ion dumping was not applied and the tungsten ions were kept trapped during observations. The visible spectra were observed with a commercial Czerny-Turner type of spectrometer. A 300-mm^{-1} grating blazed at 500 nm was used for wide range observations, whereas a 1200-mm^{-1} grating blazed at 400 nm was used for wavelength determination. The data acquisition time was typically 20 min for wide range observations with the 300-mm^{-1} grating, and 40 min for high-resolution observations with the 1200-mm^{-1} grating. Wavelength calibration was done by using emission lines from several standard lamps placed outside CoBIT. The uncertainty in the wavelength calibration was estimated from reproducibility to be about ± 0.05 nm.

III. THEORETICAL CALCULATION

A CR model is developed for individual W^{8+} and W^{9+} ions using FAC version 1.1.5 [20]. In the CR model, we assume that

TABLE I. List of configurations considered in configuration interaction in FAC.

W^{8+}	W^{9+}
$5s^2 4f^{14} 5p^4$	$5s^2 4f^{14} 5p^3$
$5s^2 4f^{13} 5p^5$	$5s^2 4f^{13} 5p^4$
$5s^2 4f^{12} 5p^6$	$5s^2 4f^{12} 5p^5$
$5s^1 4f^{14} 5p^5$	$5s^2 4f^{11} 5p^6$
$5s^1 4f^{13} 5p^6$	$5s^1 4f^{14} 5p^4$
$5s^2 4f^{14} 5p^3 5(d, f)$	$5s^1 4f^{13} 5p^5$
$5s^2 4f^{13} 5p^4 5(d, f)$	$5s^1 4f^{12} 5p^6$
$5s^2 4f^{12} 5p^5 5(d, f)$	$5s^2 4f^{14} 5p^2 5(d, f)$
$5s^2 4f^{11} 5p^6 5(d, f)$	$5s^2 4f^{13} 5p^3 5(d, f)$
$5s^1 4f^{14} 5p^4 5(d, f)$	$5s^2 4f^{12} 5p^4 5(d, f)$
$5s^1 4f^{13} 5p^5 5(d, f)$	$5s^2 4f^{11} 5p^5 5(d, f)$
$5s^1 4f^{12} 5p^6 5(d, f)$	$5s^2 4f^{10} 5p^6 5(d, f)$
	$5s^1 4f^{14} 5p^3 5(d, f)$
	$5s^1 4f^{13} 5p^4 5(d, f)$
	$5s^1 4f^{12} 5p^5 5(d, f)$

the various levels of the ions are interconnected through only collisional and radiative processes in the plasma. In the EBIT plasma, electron density is low, typically $10^{10}\text{--}10^{12}\text{ cm}^{-3}$, and in the present case the electron-beam energy is less than the ionization energy of W^{8+} and W^{9+} ; on that note, we neglect various recombination processes such as three-body recombination and dielectronic recombination. In the present model, we consider the level population or depopulation by electron excitation, deexcitation, ionization, and radiative decay. In the steady state, for an excited level the rate balance equation with the normalization condition $\sum_j n_j = 1$ is given by

$$\sum_{\substack{i \\ i \neq j}} k_{ij} n_i n_e + \sum_{i>j} A_{ij} n_i - \sum_{\substack{i \\ i \neq j}} k_{ji} n_j n_e - \sum_{i<j} A_{ji} n_j - n_j n_e k_{j+} = 0.$$

Here, k_{ij} , A_{ij} , n_j , and n_e are the electron impact excitation (deexcitation) rate coefficients, the transition probability from level $i \rightarrow j$, the population of the j th level, and the electron density, respectively. Electron excitation rates are obtained by integrating the cross section with the product of a narrow Gaussian electron energy distribution function with a 5-eV full width at half maximum as an EBIT with monoenergetic electrons. Deexcitation rates are obtained by the principle of detailed balance from excitation rates. In the present model, for W^{8+} a total of 4418 levels and ionization levels generated from excitation from the reference $4f^{14} 5p^4$, $4f^{13} 5p^5$, and $4f^{12} 5p^6$ configurations to $5d$ and $5f$ and, for W^{9+} , a total of 14 639 levels by excitation from $4f^{14} 5p^3$, $4f^{13} 5p^4$, $4f^{12} 5p^5$, and $4f^{11} 5p^6$ to $5d$ and $5f$ are considered as shown in Table I. In total more than 1×10^6 cross sections among all the states and millions of radiative decay channels (E1, E2, E3, M1, M2, and M3) for W^{8+} and W^{9+} are accounted for in the model. All the atomic data for energy levels, transition probabilities, and cross sections are calculated using the wave function ob-

TABLE II. List of configurations used in active set for W^{8+} and W^{9+} in CI calculations from GRASP2018.

Configurations	CSFs
W^{8+}	
DF + (5d, 5f, 5g) _{SD}	141 657
DF + (5d, 5f, 5g) _{SD} + (6s, 6p, 6d, 6f) _{SD}	485 857
DF + (5d, 5f, 5g) _{SD} + (6s, 6p, 6d, 6f) _{SD} + (7s, 7p, 7d, 7f) _S	488 622
W^{9+}	
DF + (5d, 5f, 5g) _{SD}	630 254
DF + (5d, 5f, 5g) _{SD} + (6s, 6p, 6d, 6f) _{SD}	799 959
DF + (5d, 5f, 5g) _{SD} + (6s, 6p, 6d, 6f) _{SD} + (7s, 7p, 7d, 7f) _S	811 309

tained within the relativistic configurational-interaction (RCI) method using FAC 1.1.5. The rate equations for all the considered levels are solved simultaneously to obtain the level populations and intensity ($I = E_{ij}A_{ij}n_j$). Spectra are obtained from line convolution with Gaussian functions having a standard deviation of 0.1 eV.

In FAC, the basis wave functions to calculate all the atomic properties are obtained from a single potential representing the screening of nuclear potential. The potential is optimized to the average electron clouds of configurations, which results in the less optimized potential for individuals. The average energies of each configuration group with the individually optimized potential and under the potential taking into account all configuration groups are obtained, and the difference between the two is used to adjust the final energy levels [20]. Further improvement is made by recalculating the average energy of each configuration under the radial potential obtained from a mean configuration (usually ground-state configuration) from the OPTIMIZERADIAL module. The diagonal elements of the Hamiltonian calculated in the structure module are then adjusted by the difference of the two average energies for each configuration. In the present case, for W^{8+} and W^{9+} , including the mean average configuration corrections using $4f^{14}5p^4$, $4f^{13}5p^5$, $4f^{12}5p^6$ and $4f^{14}5p^3$, $4f^{13}5p^4$, $4f^{12}5p^5$ configurations, respectively, improves the level energies and level ordering matches with the GRASP calculations. However, the inclusion of the mean average configuration corrections decreases the accuracy in level splitting between individual configuration levels. It is found that the level energies of a few lower levels are extremely sensitive to optimized potential due to substantial overlapping of levels from the reference configuration.

Moreover, in the present RCI calculation, we have included the correlation effects only via important configurational interaction (which gives the best match to the experiment) to manage the model size as it includes calculation of a vast amount of collisional cross-section and decay probability data. Further, relativistic corrections from Breit interaction in the zero-energy limit for the exchanged photon and higher-order QED effects such as self-energy and vacuum polarization are added in a subsequent (RCI) calculation.

To ensure line identification from the CR model, we have also performed the MCDF calculations using GRASP2018 [5]. We have calculated the energy of the first 30 and 144 lowest levels and transition probabilities for M1 transitions in W^{8+} and W^{9+} , respectively. In MCDF approximation, the wave function for an atomic state is approximated by an atomic state function (ASF), which can be expressed as a linear

combination of configuration state functions (CSFs), which have the same angular momentum J and parity P [21,24]:

$$\Psi(\Gamma PJ) = \sum_{i=1}^n C_i \phi(\Gamma_i PJ).$$

Here, ϕ_i are the CSFs given as antisymmetric products of the one-electron Dirac-Fock orbitals (Slater determinant). ($\Gamma_i PJ$) represents all information required to uniquely define the CSFs such as orbital occupation numbers, coupling, etc. n denotes the number of CSFs included in the expansion, and C_i denotes the mixing coefficients. To obtain the final ASFs, we start with wave-function calculation for multireference using a self-consistent-field (SCF) procedure based on the Dirac-Coulomb Hamiltonian and various correlation effects by including more CSFs layer by layer using an active set approach [22,23]. Moreover, corrections from the Breit interaction, i.e., transverse photon interaction in the low-frequency limit and the higher-order QED modifications due to self-energy correction and vacuum polarization (within a screened hydrogenic approximation), are added in RCI calculations [25,26].

Present systems W^{8+} and W^{9+} are near neutral ions having three holes and four holes, respectively, with $4f$ and $5p$ open orbitals. For these ions getting the convergence for the spectroscopic orbitals in the SCF procedure is very difficult. No convergence is found using initial estimation such as screened hydrogenic functions and the Thomas-Fermi model. Therefore, first, we have used the DBSR_{HF} program [27] to generate orbital wave functions and used these as GRASP input for initial guess in SCF. DBSR is a B-spline version of a general Dirac-Hartree-Fock program. Then for all level calculation of the levels from reference configurations (for W^{8+} $5s^2 4f^m 5p^n$, $m+n=18$, and for W^{9+} $5s^2 4f^m 5p^n$, $m+n=17$) we include valence-valence and partial core-valence correlation effects via single double (SD) excitation from core valence to active set space. In the present calculation, all electrons are divided into two parts; electrons in $5p$ and $4f$ orbitals are taken as valence electrons and in other inner orbitals as core electrons. Correspondingly, the correlation is taken as the interaction between the valence electrons and valence electrons with core electrons. In the present calculation, convergence is obtained by the following approach: we add the active set space in the multireference DF calculation layer by layer via SD excitation from $5s$, $4f$, and $5p$ with a restriction that only one electron can excite from $5s$ at a time. While optimizing the outer layer, all the inner layers are fixed. We expanded the active set in Table II.

In the case of W^{9+} , CSF expansion was too large, so we set restrictions that orbitals in the active space are always

TABLE III. Experimental and theoretical wavelengths (in nm) and theoretical transition probabilities A (s^{-1}) for transitions in Dy-like W^{8+} .

Label	Upper level	Lower level	λ_{exp}	λ_{th}				A		
				FAC	GRASP1	GRASP2	[6]	FAC	GRASP1	GRASP2
a	$[(4\bar{f}^5 4f^8)_{5/2}(5\bar{p}^2 5p^3)_{3/2}]_4$	$[(4\bar{f}^6 4f^7)_{7/2}(5\bar{p}^2 5p^3)_{3/2}]_5$	431.78	416.43	434.04	432.84	420.84	1.76×10^2	1.70×10^2	1.70×10^2
b	$[(4\bar{f}^4 4f^8)_{4/2}(5\bar{p}^2 5p^4)_{0/2}]_4$	$[(4\bar{f}^5 4f^7)_{5/2}(5\bar{p}^2 5p^4)_{0/2}]_5$	447.14	440.71	433.31	443.31		1.42×10^2	1.73×10^2	1.59×10^2
c	$[(4\bar{f}^5 4f^8)_{5/2}(5\bar{p}^2 5p^3)_{3/2}]_2$	$[(4\bar{f}^6 4f^7)_{7/2}(5\bar{p}^2 5p^3)_{3/2}]_3$	477.29	460.07	482.16	476.68	459.67	9.47×10^1	9.13×10^1	9.30×10^1
d	$[(4\bar{f}^5 4f^7)_{3/2}(5\bar{p}^2 5p^4)_{0/2}]_3$	$[(4\bar{f}^6 4f^6)_{4/2}(5\bar{p}^2 5p^4)_{0/2}]_4$	570.52	556.32	544.50	571.25	546.24	8.22×10^1	9.06×10^1	8.45×10^1
e	$[(4\bar{f}^5 4f^7)_{5/2}(5\bar{p}^2 5p^4)_{0/2}]_5$	$[(4\bar{f}^6 4f^6)_{6/2}(5\bar{p}^2 5p^4)_{0/2}]_6$	611.17	614.72	604.75	619.74	596.24	1.05×10^2	1.18×10^2	1.10×10^2

doubly excited. Here, we have treated valence-valence and core-valence correlation via including CSFs generated from single and double excitation only from $5s$, $4f$, and $5p$ orbitals. Sometimes deep core correlation by excitation from inner orbitals may also give some accountable contribution [22,23]. However, due to complex and large expansion sets (even taking excitation only from $5s$, $4f$, and $5p$), we did not include excitation from the inner core in RCI because of computational restrictions. Nevertheless, this approach can provide accuracy in transition energies for line identification in the visible range, as shown in Tables III and IV.

IV. RESULTS AND DISCUSSION

In Fig. 2, experimental spectra observed with a 300-mm⁻¹ grating are shown at various electron-beam energies from 90 to 130 eV in the visible region, and the lines presented at 130 eV are assigned to transitions in W^{8+} and W^{9+} . Since an EBIT has monoenergetic electrons, only those ionic states for which electron energy is higher than the ionization energy should be presented in the plasma. However, due to the excitation from metastable states, ions can be generated at an electron-beam energy lower than the ionization threshold.

In the present case, it can be understood as follows: ionization energy from W^{7+} is 141 eV, and from the CR model calculation various metastable levels are found in W^{7+} (from $4f^{13}5p^5d^1$ and $4f^{12}5p^6d^1$ levels) at around 40–60 eV, that explains the presence of W^{8+} even at 90 eV. In W^{8+} also there are various highly populated metastable states from $4f^{14}5p^4$, $4f^{13}5p^5$, and $4f^{12}5p^6$ (in total 80% of the population) at 3–26 eV, and a few from $4f^{13}5p^4d^1$ and $4f^{12}5p^5d^1$ at around 50–57 eV populated only 1%, and the ionization energy of W^{8+} is 160 eV, which shows the presence of W^{9+} at 130 eV. However, ionization energy for W^{9+} is 180 eV

and the population is mostly concentrated in metastable states from $4f^{14}5p^3$, $4f^{13}5p^4$, $4f^{12}5p^5$, and $4f^{11}5p^6$ configurations situated up to 28 eV from the ground, therefore at 130 eV the most probable lines are from W^{8+} and W^{9+} ions.

In Fig. 3, we have shown simulated spectra for W^{8+} and W^{9+} at electron energy 130 eV and electron density 10^{10} cm⁻³ along with experimental spectra recorded at 130 eV. This shows that spectral features from the model are similar to experimentally observed spectra, which allows us to identify the lines. From the CR model calculations, the observed lines are assigned as magnetic dipole (M1) transitions belonging to intratransition between levels of $4f^{13}5p^5$ and $4f^{12}5p^6$ configurations in W^{8+} and $4f^{13}5p^4$ and $4f^{12}5p^5$ in W^{9+} ion.

The experimental wavelength of newly identified lines for W^{8+} and W^{9+} , along with theoretical values from FAC and GRASP, are presented in Tables III and IV, respectively. Theoretically calculated transition probabilities are also given in the same tables. Levels are represented in j - j coupled notation, where $n\bar{l}$ and nl correspond to the shell with total angular momentum $j = l - 1/2$ and $l + 1/2$, respectively. Lowest-energy levels from the reference configuration in W^{8+} and W^{9+} and identified transitions (labeled as a, b, etc.) are presented in Figs. 4 and 5. Here, GRASP1 and GRASP2 represent DF + CI calculation only with reference configurations and including active space core-valence correlation corrections, respectively. For W^{8+} in Table III, we have compared the present wavelengths with the CI calculations of Berengut *et al.* [6]. It can be seen that theoretical values predicted from GRASP2 are more close to the measured wavelengths, and values reported [6] are similar to present FAC values. However, the difference between the transition energies reported in [6] and current theoretical values obtained from GRASP is within the 6000 cm⁻¹ uncertainty claimed in [6]. For W^{9+} , there

TABLE IV. Experimental and theoretical wavelengths (in nm) and theoretical transition probabilities A (s^{-1}) for transitions in Tb-like W^{9+} .

Label	Upper level	Lower level	λ_{exp}	λ_{th}			A		
				FAC	GRASP1	GRASP2	FAC	GRASP1	GRASP2
k	$[(4\bar{f}^5 4f^8)_{5/2}(5\bar{p}^2 5p^2)_{2/2}]_{7/2}$	$[(4\bar{f}^6 4f^7)_{7/2}(5\bar{p}^2 5p^2)_{2/2}]_{9/2}$	409.66	398.65	427.35	408.19	1.17×10^2	1.38×10^2	1.30×10^2
l	$[(4\bar{f}^5 4f^8)_{5/2}(5\bar{p}^2 5p^2)_{2/2}]_{9/2}$	$[(4\bar{f}^6 4f^7)_{7/2}(5\bar{p}^2 5p^2)_{2/2}]_{11/2}$	438.68	424.41	450.71	442.33	1.68×10^2	1.85×10^2	1.78×10^2
m	$[(4\bar{f}^5 4f^7)_{5/2}(5\bar{p}^2 5p^3)_{3/2}]_{13/2}$	$[(4\bar{f}^6 4f^6)_{6/2}(5\bar{p}^2 5p^3)_{3/2}]_{15/2}$	481.55	478.78	477.74	483.71	2.25×10^2	2.21×10^2	2.17×10^2
n	$[(4\bar{f}^5 4f^8)_{5/2}(5\bar{p}^2 5p^2)_{0/2}]_{5/2}$	$[(4\bar{f}^6 4f^7)_{7/2}(5\bar{p}^2 5p^2)_{0/2}]_{7/2}$	533.20	514.88	555.06	536.70	1.16×10^2	1.30×10^2	1.25×10^2
o	$[(4\bar{f}^5 4f^7)_{5/2}(5\bar{p}^2 5p^3)_{3/2}]_{11/2}$	$[(4\bar{f}^6 4f^6)_{6/2}(5\bar{p}^2 5p^3)_{3/2}]_{13/2}$	608.41	596.08	590.63	604.53	1.16×10^2	1.13×10^2	1.11×10^2

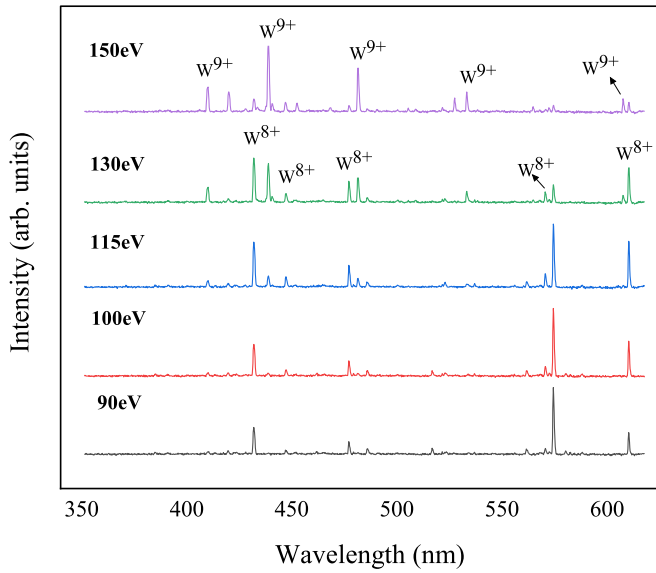


FIG. 2. Experimental spectra of tungsten ions in the visible range obtained with a compact electron-beam ion trap at various electron-beam energies (written at the right side of the respective spectra).

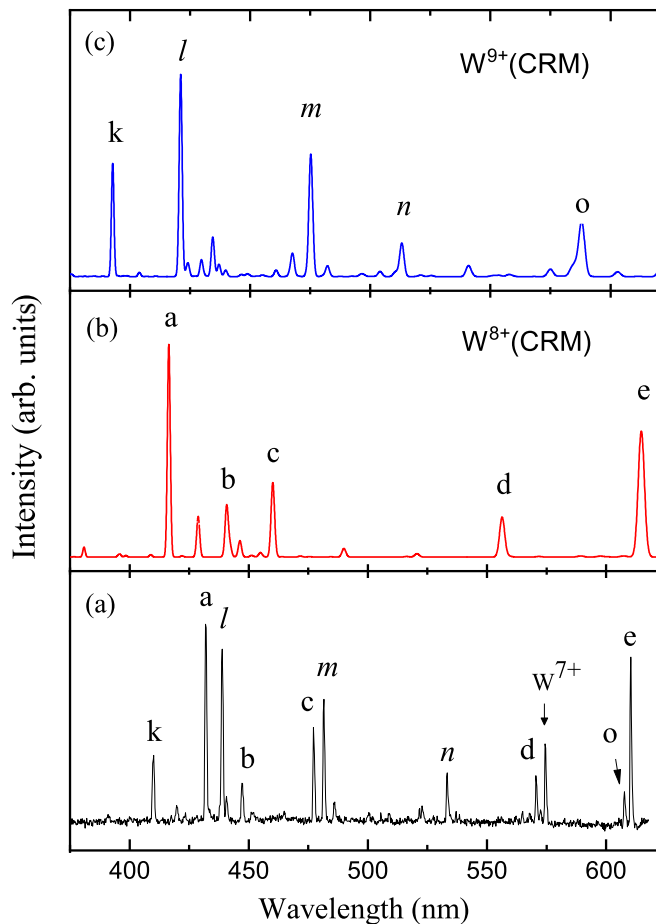


FIG. 3. Experimental (a) and simulated (b, c) spectra of W^{8+} and W^{9+} ions, respectively, in the visible range at electron-beam energy 130 eV. The simulated spectra are obtained by CRM at electron density 10^{10} cm^{-3} using FAC.

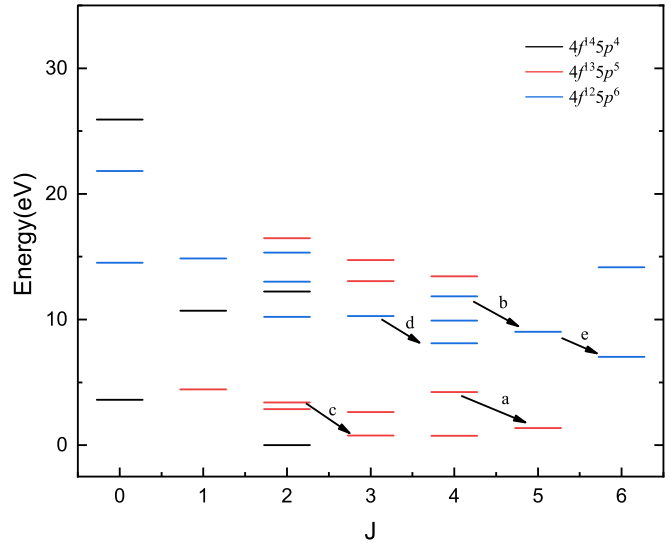


FIG. 4. Partial energy-level diagram of W^{8+} with the lowest 30 energy levels calculated from GRASP2018. Different colors show levels with different cores. The vertical axis shows energy with respect to ground state $4f^{14}5p^4$ ($J = 2$), and the horizontal axis shows total angular momentum. The arrow represents the M1 transition identified in Table III.

are no previous experimental or theoretical data for transition wavelength or probability available for comparison with present values.

Table III shows that for W^{8+} the theoretical wavelengths obtained from FAC are shifted in spectra with a maximum difference from the experimental value of 4%. Moreover, to ensure the identification, we have also compared FAC results with MCDF calculations from GRASP. From the difference

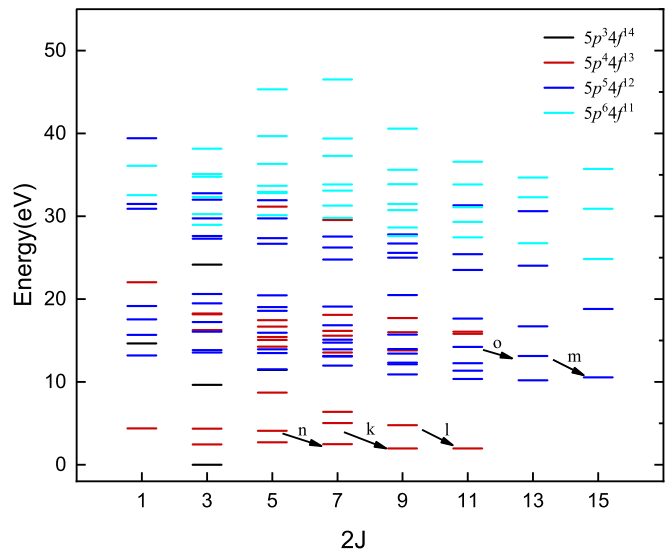


FIG. 5. Partial energy-level diagram of W^{9+} with the lowest 144 energy levels calculated from GRASP2018. Different colors show levels with different cores. The vertical axis shows energy with respect to ground state $4f^{14}5p^3$ ($J = 3/2$), and the horizontal axis shows total angular momentum ($2J$). The arrow represents the M1 transition identified in Table IV.

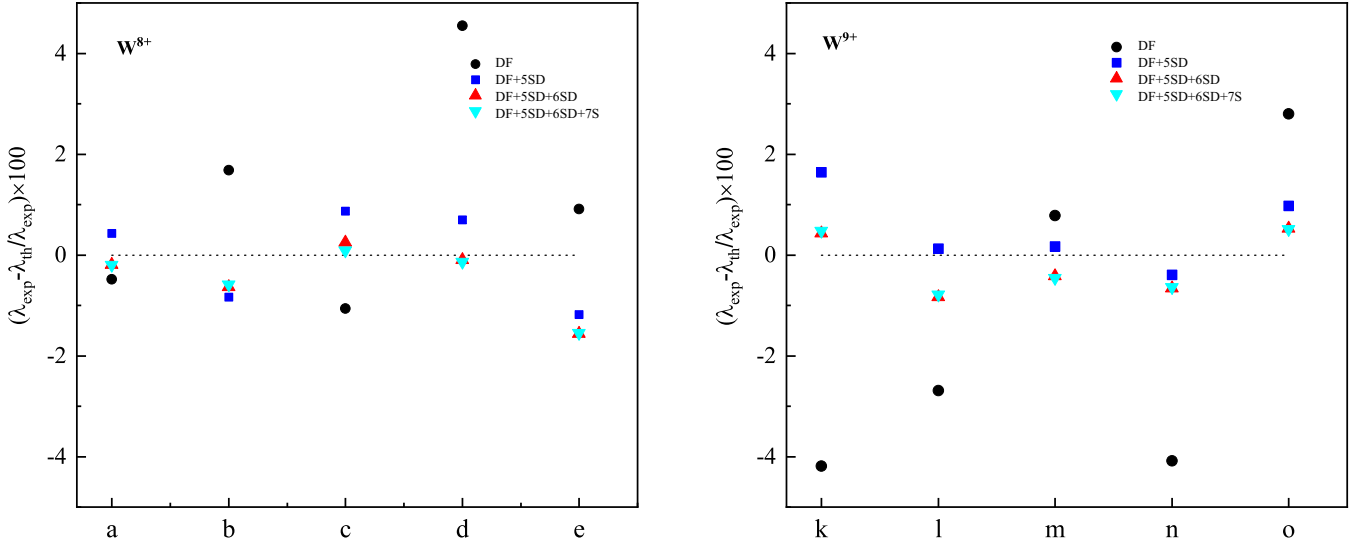


FIG. 6. Relative deviation in wavelengths obtained from GRASP (for each expansion set) to the experimental wavelength for lines labeled in Tables III and IV.

between GRASP1 and GRASP2 wavelengths, it is clear that there is a significant contribution from the different correlations of the orbitals. The relative change in the transition wavelengths by adding active set expansion up to $(5d, 5f, 5g)_{SD}$ maximum 4% and further adding expansion up to $(6s, 6p, 6d, 6f)_{SD}$ and $(7s, 7p, 7d, 7f)_{SD}$ changes the wavelength by less than 1 and 0.15%, respectively. For W^{9+} , the theoretical wavelengths obtained from FAC are shifted in spectra with a maximum difference from the experimental value of 3.5%. The relative change in the transition wavelengths by adding active set expansion up to $(5d, 5f, 5g)_{SD}$ maximum 5.6% and further adding expansion up to $(6s, 6p, 6d, 6f)_{SD}$ and $(7s, 7p, 7d, 7f)_{SD}$ changes the wavelength by less than 1.2 and 0.1%, respectively. From GRASP1 and GRASP2 results and mixing coefficients, it is noticed that for W^{9+} correlation contribution is larger than for W^{8+} . These results include the Breit and QCD correction contribution in low-frequency approximation, which increases the wavelengths approximately by 4%. The relative deviation in wavelengths obtained from GRASP (for each expansion set) to the experimental wavelength is plotted in Figs. 6(a) and 6(b) for W^{8+} and W^{9+} , respectively. It shows that the expansion up to $7s, p, d,$ and f orbitals reasonably explains the correlation. It can be improved by taking the correlation effect more accurately by including core-valence correlation from inner orbital and core-core correlation. Nevertheless, present accuracy provides the line identification very well.

In the present measurements, the identified lines are M1 transitions between states of the same configuration. They do not provide information about the relative position of the states of different configurations, which is essential to make any progress towards the new generation of atomic clocks. However, such measurements are very difficult since the transitions are very weak (strongly forbidden M1 transitions or E2 transitions). For example, the E2 transition from the ground state of W^{8+} , $4f^{14}5p^4 \ ^3P_2$, to $4f^{12}5p^6 \ ^3F_4$ with large sensitivity coefficient [6] has a transition probability almost two orders lower than for the currently observed lines. Therefore,

at present, information about the relative position of the states of different configurations can be predicted from the theory only. In Tables S1 and S2 (see Supplemental Material) [28], we have tabulated level energies for lower-lying levels of W^{8+} and W^{9+} calculated from GRASP2018 corresponding to Figs. 4

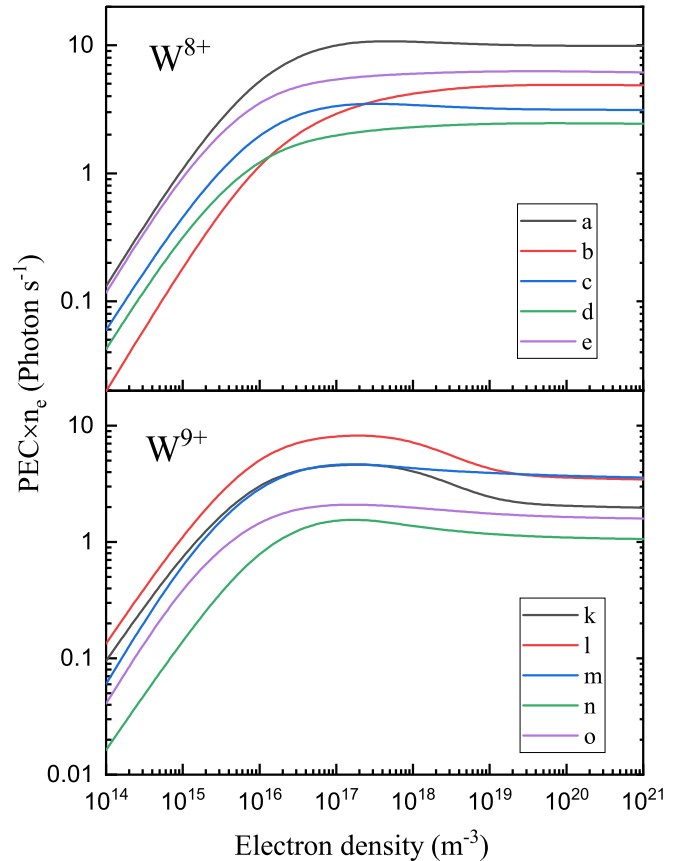


FIG. 7. Photon emission coefficient (PEC) as a function of n_e for the lines listed in Tables III and IV estimated by CRM at $Te = 40$ eV for W^{8+} and $Te = 50$ eV for W^{9+} .

and 5. However, it is hard to access the accuracy of transition energies in the absence of measurements.

Furthermore, to see the importance of the identified M1 lines of W^{8+} and W^{9+} in the fusion plasma environment, we have calculated the photon emission coefficient (PEC) at various electron densities (10^{14} – 10^{21} m^{-3}) and electron temperature 40 and 50 eV, respectively (at which W^{8+} and W^{9+} are most abundant), as shown in Fig. 7. In this case, the rate coefficients are calculated by using the Maxwellian electron energy distribution function. At higher electron density (10^{18} m^{-3}), PECs are almost independent of electron density. We found that the present lines are as strong as the M1 lines of highly charged tungsten ions including W^{26+} observed in large helical device (LHD) plasma at National Institute for Fusion Science (NIFS) [29–32] for which PECs are calculated to be the order of 10^{-18} m^3/s at $Te = 1keV$ and $n_e = 10^{19}$ m^{-3} . Based on the visible emission line, they have demonstrated the evaluation of the ion temperature in the LHD [31]. Therefore, such information for visible lines of W^{8+} – W^{9+} could be very important for ITER plasma diagnostic purposes.

V. SUMMARY

We identified additional M1 lines from W^{8+} and W^{9+} ions in the visible range. The CR model is used to identify the lines, and also identification is ensured by comparing MCDF calculations from GRASP2018. The energy-level calculations for the lower-lying levels belonging to reference states in W^{8+} and W^{9+} are obtained by including core-valence correlations in a restricted manner. However, more rigorous calculations which account for correlation effects completely can be further performed, such as for the two-hole system studied in the recent theoretical evolution by Cheung *et al.* [33]. We hope that the present results will be important in atomic structure calculations as well as very useful in fusion plasma diagnostics.

ACKNOWLEDGMENT

This work was supported by NIFS Collaboration Research Program No. NIFS17KBAF028 and NIFS20KLPF075.

-
- [1] R. J. Hawryluk *et al.*, *Nucl. Fusion* **49**, 065012 (2009).
- [2] N. J. Peacock, M. G. O’Mullane, R. Barnsley, and M. Tarbutt, *Can. J. Phys.* **86**, 277 (2008).
- [3] C. H. Skinner, *Phys. Scr. T* **134**, 014022 (2009).
- [4] J. Clementson, P. Beiersdorfer, E. W. Magee, H. S. McLean, and R. D. Wood, *J. Phys. B* **43**, 144009 (2010).
- [5] C. Froese Fischer, G. Gaigalas, P. Jönsson, and J. Bieroń, *Comput. Phys. Commun.* **237**, 184 (2019).
- [6] J. C. Berengut, V. A. Dzuba, V. V. Flambaum, and A. Ong, *Phys. Rev. Lett.* **106**, 210802 (2011).
- [7] J. C. Berengut, V. A. Dzuba, V. V. Flambaum, and A. Ong, *Phys. Rev. A* **86**, 022517 (2012).
- [8] Y. Ralchenko, *Plasma Fusion Res.* **8**, 2503024 (2013).
- [9] A. E. Kramida and T. Shirai, *At. Data Nucl. Data Tables* **95**, 305 (2009).
- [10] A. Ryabtsev, E. Kononov, R. Kildiyarova, W. Tchang-Brillet, J. F. Wyart, N. Champion, and C. Blaess, *Atoms* **3**, 273 (2015).
- [11] A. Ryabtsev, E. Y. Kononov, R. Kildiyarova, W. L. Tchang-Brillet, and J. F. Wyart, *Phys. Scr.* **87**, 045303 (2013).
- [12] M. Mita, H. A. Sakaue, D. Kato, I. Murakami, and N. Nakamura, *Atoms* **5**, 13 (2017).
- [13] Q. Lu, J. He, H. Tian, M. Li, Y. Yang, K. Yao, C. Chen, J. Xiao, J. G. Li, B. Tu, and Y. Zou, *Phys. Rev. A* **99**, 042510 (2019).
- [14] W. Li, Z. Shi, Y. Yang, J. Xiao, T. Brage, R. Hutton, and Y. Zou, *Phys. Rev. A* **91**, 062501 (2015).
- [15] A. Komatsu, J. Sakoda, M. Minoshima, H. A. Sakaue, X. B. Ding, D. Kato, I. Murakami, F. Koike, and N. Nakamura, *Plasma Fusion Res.: Rapid Commun.* **7**, 1201158 (2012).
- [16] A. Kramida, Y. Ralchenko, J. Reader, and NIST ASD Team (2019), NIST Atomic Spectra Database (version 5.7.1), <https://physics.nist.gov/asd>.
- [17] M. Mita, H. A. Sakaue, D. Kato, I. Murakami, and N. Nakamura, *J. Phys.: Conf. Ser.* **875**, 012019 (2017).
- [18] N. Nakamura, H. Kikuchi, H. A. Sakaue, and T. Watanabe, *Rev. Sci. Instrum.* **79**, 063104 (2008).
- [19] Y. Kobayashi, K. Kubota, K. Omote, A. Komatsu, J. Sakoda, M. Minoshima, D. Kato, J. Li, H. A. Sakaue, I. Murakami, and N. Nakamura, *Phys. Rev. A* **92**, 022510 (2015).
- [20] M. F. Gu, *Can. J. Phys.* **86**, 675 (2008).
- [21] I. P. Grant, B. J. McKenzie, P. H. Norrington, D. F. Mayers, and N. C. Pyper, *Comput. Phys. Commun.* **21**, 207 (1980).
- [22] X. L. Guo, R. Si, S. Li, M. Huang, R. Hutton, Y. S. Wang, C. Y. Chen, Y. M. Zou, K. Wang, J. Yan, C. Y. Li, and T. Brage, *Phys. Rev. A* **93**, 012513 (2016).
- [23] Z. Fei, W. Li, J. Grumer, Z. Shi, R. Zhao, T. Brage, S. Huldt, K. Yao, R. Hutton, and Y. Zou, *Phys. Rev. A* **90**, 052517 (2014).
- [24] J. Olsen, B. O. Roos, P. Jørgensen, and H. Jørgen Aa. Jensen, *J. Chem. Phys.* **89**, 2185 (1988).
- [25] P. J. Mohr, *Phys. Rev. A* **26**, 2338 (1982).
- [26] B. J. McKenzie, I. P. Grant, and P. H. Norrington, *Comput. Phys. Commun.* **21**, 233 (1980).
- [27] O. Zatsarinny and C. F. Fischer, *Comput. Phys. Commun.* **202**, 287 (2016).
- [28] See Supplemental Material at <http://link.aps.org/supplemental/10.1103/PhysRevA.102.042818> for energy levels of lower-lying states of W^{8+} and W^{9+} calculated from GRASP2018.
- [29] D. Kato *et al.*, *Phys. Scr. T* **156**, 014081 (2013).
- [30] M. Shinohara, K. Fujii, D. Kato, N. Nakamura, M. Goto, S. Morita, M. Hasuo, and LHD Experiment Group, *Phys. Scr.* **90**, 125402 (2015).
- [31] K. Fujii, Y. Takahashi, Y. Nakai, D. Kato, M. Goto, S. Morita, M. Hasuo, and LHD Experiment Group, *Phys. Scr.* **90**, 125403 (2015).
- [32] K. Fujii, D. Kato, N. Nakamura, M. Goto, S. Morita, and M. Hasuo, *J. Phys. B* **50**, 055004 (2017).
- [33] C. Cheung, M. S. Safronova, S. G. Porsev, M. G. Kozlov, I. I. Tupitsyn, and A. I. Bondarev, *Phys. Rev. Lett.* **124**, 163001 (2020).